RSC Advances

COMMUNICATION

View Article Online
View Journal | View Issue

Cite this: *RSC Adv.*, 2016, **6**, 67372

Received 7th June 2016
Accepted 10th July 2016

DOI: 10.1039/c6ra14799b

www.rsc.org/advances

N-Heterotriangulene chromophores with 4-pyridyl anchors for dye-sensitized solar cells†

Ute Meinhardt,[a] Fabian Lodermeyer,[b] Tobias A. Schaub,[a] Andreas Kunzmann,[b] Pavlo O. Dral,[c] Anna Chiara Sale,[a] Frank Hampel,[a] Dirk M. Guldi,*[b] Ruben D. Costa*[b] and Milan Kivala*[a]

A series of dimethylmethylene-bridged *N*-heterotriangulenes decorated with one, two, and three electron-withdrawing 4-pyridyls were synthesized. Their photophysical and electrochemical characteristics were examined and their successful application in n-type TiO_2- and ZnO-based dye-sensitized solar cells demonstrated the ability of the 4-pyridyl moiety to act as an anchor.

Starting with the pioneering work by Grätzel and co-workers, dye-sensitized solar cells (DSSCs),[1] turned into frontrunners towards the development of environmentally benign energy sources.[2] One of the biggest challenges in the field, that is, academic and industrial research, constitutes the development of metal-free organic sensitizers as an alternative to ruthenium-based dyes. Here, their low-cost syntheses, their high molar extinction coefficients, and the possibility to efficiently control their electronic and molecular structures through molecular design are important assets, which have fueled the research in this field during recent years.[3] Most of the organic dyes with an electron donor–π-bridge–acceptor (D–π–A) architecture feature broad and intense absorptions in the visible region of the solar spectrum as a consequence of an intramolecular charge-transfer (ICT).[4] Numerous types based on organic electron donors, such as indoline,[5] thiophene,[6] dithiafulvene,[7] 4*H*-pyran-4-ylidene,[8] in general, and, triphenylamine,[9,10] in particular, have been developed and applied in DSSCs. Notably, dimethylmethylene-bridged triphenylamine (**DTPA**), so-called *N*-heterotriangulene,[11] has only recently been employed as an electron donor part in dyes with enhanced photovoltaic performances.[12] Vital for the performance is the planarization of the originally propeller-shaped triphenylamine.

The acceptor part most often consists of a carboxylic or cyanoacrylic acid as anchor to ensure efficient electronic communication through the formation of a strong bidentate linkage with Brønsted acid sites at the TiO_2 surface.[3,4,13] Recently, an electron-withdrawing 4-pyridyl has been reported by Ooyama and co-workers as an alternative anchor.[14] It enables efficient electron injection upon forming strong coordinative bonds with the Lewis acidic sites at the TiO_2 surface.[15] Since then, pyridyl linkers have been combined with a variety of electron donors such as carbazole,[16] porphyrins,[17] boron-dipyrromethene,[18] tetrahydroquinoline,[19] and triphenylamine.[20]

To our surprise, organic sensitizers combining *N*-heterotriangulene donors with pyridyl anchoring moieties have not been reported to date. As part of our ongoing research on functional molecules and materials based on *N*-heterotriangulenes,[21] we have designed and synthesized a series of dimethylmethylene-bridged *N*-heterotriangulenes decorated with one, two, and three electron-withdrawing 4-pyridyl anchoring groups. The resulting electron donor–acceptor dyes were studied regarding their photophysical and electrochemical properties, as well as their integration into DSSCs featuring TiO_2 and ZnO electrodes.

For the synthesis of mono-**1**, bis-**2**, and tris-pyridyl *N*-heterotriangulene **3**, the corresponding brominated precursors, prepared by treatment of the parent **DTPA** with an appropriate amount of *N*-bromosuccinimide,[22,23] were subjected to Pd-catalyzed Suzuki–Miyaura cross-coupling reaction with 4-pyridylboronic acid under microwave irradiation (Fig. 1; for experimental details, see ESI†). The target compounds **1–3** were isolated in good yields between 55% (**1**), and 86% (**3**) as orange solids. They are stable under ambient conditions and soluble in common organic solvents. The chemical identity of **1–3** was confirmed by ^1H and ^{13}C NMR spectroscopy, high resolution mass spectrometry, and elemental analysis (see ESI†).

[a]*Department of Chemistry and Pharmacy, Friedrich-Alexander University Erlangen-Nürnberg, Henkestraße 42, 91054 Erlangen, Germany. E-mail: milan.kivala@fau.de*

[b]*Department of Chemistry and Pharmacy, Friedrich-Alexander University Erlangen-Nürnberg, Egerlandstraße 3, 91058 Erlangen, Germany. E-mail: dirk.guldi@fau.de; ruben.costa@fau.de*

[c]*Max-Planck-Institut für Kohlenforschung, Kaiser-Wilhelm-Platz 1, 45470 Mülheim an der Ruhr, Germany*

† Electronic supplementary information (ESI) available. CCDC 1441546. For ESI and crystallographic data in CIF or other electronic format see DOI: 10.1039/c6ra14799b

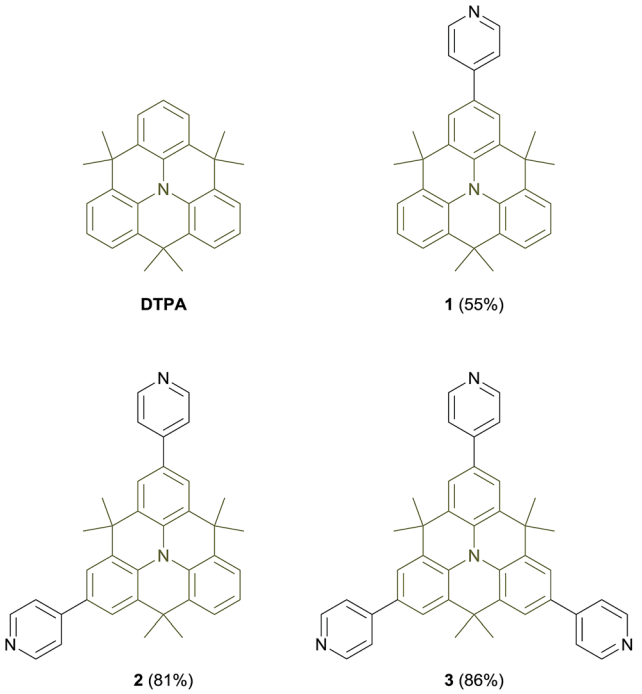

Fig. 1 Chemical structures of *N*-heterotriangulene (DTPA) and mono-**1**, bis-**2**, and trispyridyl substituted dyes **3**; in brackets, the yields of the Suzuki–Miyaura cross-coupling reaction between 4-pyridylboronic acid and the corresponding brominated DTPA are shown.

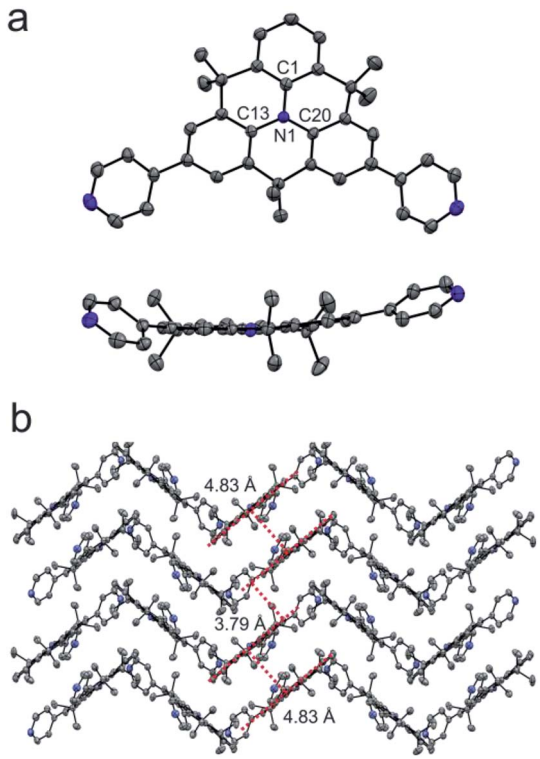

Fig. 2 (a) Molecular structure of **2** (top and side view, 50% probability level, H-atoms are omitted for clarity). (b) Illustration of the herringbone packing of **2** with alternating distances of the individual layers.

Single crystals of **2** suitable for X-ray crystallographic analysis were grown by slow evaporation of a solution of **2** in CH_2Cl_2/MeOH at room temperature. While the central 'C_3N' amine motif appears to be virtually planar with the sum of C–N–C angles of 359.5°, the flexibility of the C(sp^3)-bridges enables slightly bent molecular geometry in the solid state in analogy to the parent **DTPA** (Fig. 2a).[22] Taking the moderate torsion angles of 29.1° and 43.8° between the two pyridine rings of **2** and the *N*-heterotriangulene framework (defined by the plane passing through C1/C13/C20/N1) into account, considerable electronic communication between the electron-donating *N*-heterotriangulene and the electron-withdrawing 4-pyridyls can be anticipated. In the crystal packing, efficient π–π stacking is prevented by the tetrahedral dimethylmethylene bridges. Such a steric hindrance leads to a herringbone arrangement with alternating distances of the individual layers of 3.79 and 4.83 Å and a tilt angle of 79.1° between individual molecules in adjacent stacks (Fig. 2b). The observed packing motif is predominantly governed by multiple C(sp^3)–H/π interactions[24] and hydrogen bonding interactions involving pyridinic nitrogens and those hydrogens of methyl and aryl groups (see ESI Fig. S7†).

The UV/vis absorption and emission spectra of **DTPA** and **1–3** in CH_2Cl_2 at room temperature are shown in Fig. 3a and their spectral data are summarized in Table 1. In contrast to the parent **DTPA**, which only exhibits a single absorption feature at 298 nm, **1–3** display two absorption bands with maxima in the range of 301–330 and 364–376 nm. The underlying electronic transitions are ascribed to π–π* transitions and ICT transitions from the central *N*-heterotriangulene as electron donor to the peripheral pyridyls as electron acceptors, respectively.[14] Notable, the introduction of the first and the second 4-pyridyl unit into the parent *N*-heterotriangulene framework leads to significant bathochromic shifts. In contrast, the attachment of the third electron-withdrawing pyridyl has only marginal impact on the spectral features. Compounds **1–3** display strong emission with maxima between 439 and 448 nm. Interestingly, a pronounced positive solvatochromism is observed in the emission spectra when going from cyclohexane to methanol with shifts ($\Delta\lambda_{em}$) of 59 nm for **1**, 63 nm for **2**, and 74 nm for **3** (Fig. 3b, see also ESI Fig. S8–S10†).[25] Protonation of the peripheral pyridyls with, for example, trifluoroacetic acid in CH_2Cl_2 leads to a strong bathochromic shift of both the absorption and the emission for **1–3** (see ESI Fig. S11 and S12†).[26] This effect is strongest for **1**, showing an absorption maximum shift ($\Delta\lambda_{abs}$) of 126 nm and an emission maximum shift ($\Delta\lambda_{em}$) of 182 nm compared to those of **2** ($\Delta\lambda_{abs}$ 109 nm, $\Delta\lambda_{em}$ 159 nm) and **3** ($\Delta\lambda_{abs}$ 81 nm, $\Delta\lambda_{em}$ 140 nm).

Cyclic voltammetry studies of **DTPA** and **1–3** in CH_2Cl_2 (with 0.1 M nBu_4NPF_6, scan rate 150 mV s^{-1}, *vs.* Fc/Fc^+) at room temperature reveal reversible one-electron oxidations in all cases. In accordance with the electron-withdrawing nature of the pyridyl substituents the oxidation potential ($E^{ox}_{1/2}$) increases as a function of the number of attached pyridyl units from unsubstituted **DTPA** (+0.36 V) to **1** (+0.42 V), to **2** (+0.50 V), and to **3** (+0.56 V). This trend is nicely corroborated in density functional theory (DFT) calculations, that is, the calculated

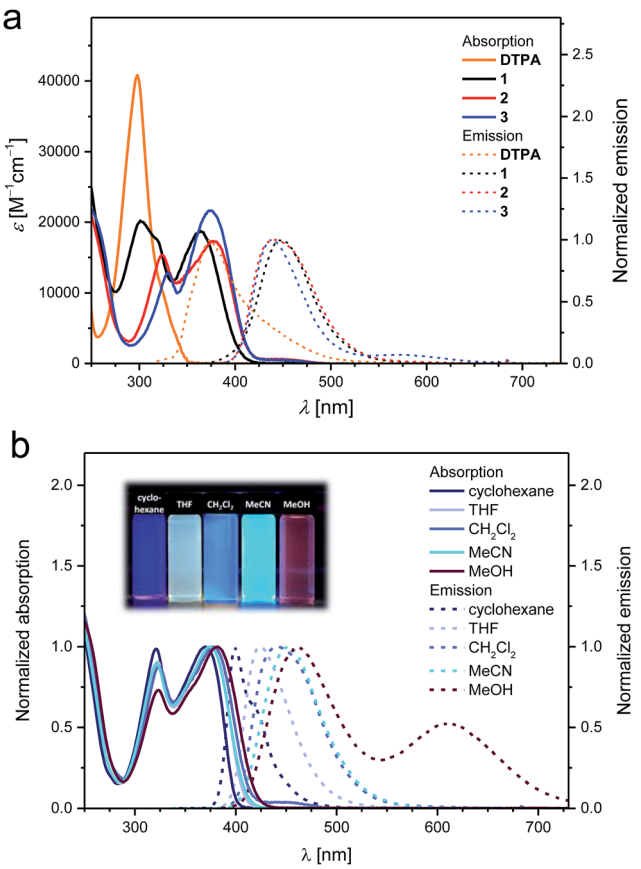

Fig. 3 (a) UV/vis absorption (solid lines) and emission spectra (dashed lines) of **DTPA**, mono-**1**, bis-**2**, and trispyridyl substituted *N*-heterotriangulene **3** in CH_2Cl_2 at room temperature (**DTPA**: λ_{exc} = 298 nm, **1**: λ_{exc} = 335 nm, **2**: λ_{exc} = 339 nm, **3**: λ_{exc} = 340 nm). (b) Exemplary normalized absorption (solid lines) and emission spectra (dashed lines) spectra of **2** measured in different solvents (cyclohexane: λ_{exc} = 315 nm, THF: λ_{exc} = 318 nm, CH_2Cl_2: λ_{exc} = 335 nm, MeCN: λ_{exc} = 313 nm, MeOH: λ_{exc} = 363 nm).

highest-occupied molecular orbital (HOMO) and lowest-unoccupied molecular orbital (LUMO) energies. They are all stabilized upon increasing the number of the pyridyl groups. The calculated Kohn–Sham frontier molecular orbital energies correlate with those estimated from the experimental data (see Table 1 and ESI Fig. S18†). In fact, the LUMO energies experience a more pronounced stabilization upon increasing the number of the electron-withdrawing pyridyls, when compared to the HOMO energies. It is worth mentioning that in all cases the LUMO energy is well above the conduction band of TiO_2 (−4.3 eV) and ZnO (−4.7 eV) ensuring a sufficient driving force for electron injection.[28]

Considering all of the above-mentioned in concert, we investigated **1–3** as sensitizers for n-type DSSCs based on TiO_2- and ZnO-based electrodes (for details regarding device fabrication and characterization, see ESI†). Interestingly, several groups have recently employed pyridyls as anchors for TiO_2-based DSSCs,[13–20] but, to the best of our knowledge, there are no examples in ZnO-based DSSCs.[2b,13] This might relate to a number of intrinsic drawbacks associated with this type of linker. On one hand, it is the slow adsorption onto the electrode surface, leading to a low dye loading compared to their carboxylic acid congeners, and, on the other hand, the rather moderate electron injection rate.[13] As a matter of fact, the latter factor is impacted by the number of pyridyls attached to the dye and the type of electrode.

As a first insight, the adsorption kinetics of **1–3** onto transparent TiO_2 electrodes were monitored by means of absorption spectroscopy. Time-dependent adsorption assays reveal the growth of the absorption around 375 nm, which is similar to the spectral features observed for **1–3** in ethanol (see ESI Fig. S13†). Nevertheless, the absorption spectra of **1–3** on TiO_2 electrodes indicate a slight red-shift and a broadening compared to the data in solution (see ESI Fig. S13†). From the latter we conclude good electronic communication between the electrode and **1–3**.[3,13,14] A direct comparison of the adsorption kinetics prompts to the fact that the number of pyridyl groups only slightly affects the time required for a complete electrode surface coverage, that is, *ca.* 30 h (see ESI Fig. S14†). As expected, the device performance relates to the adsorption time (Fig. 4). In particular, the fill factor (FF) gradually increases regardless of the number of pyridyl groups, reaching values of around 0.50 for **1**

Table 1 Photophysical and electrochemical data and HOMO and LUMO energy levels of **DTPA** and **1–3**, as well as the figures-of-merit of DSSCs with **1–3**

Dye	λ_{abs}[a] [nm], (ε [M^{-1} cm^{-1}])	λ_{em}[a] [nm]	Stokes shift[a] [cm^{-1}]	$E_{1/2}^{ox}$[b] [V]	HOMO[c], (theo.)[d] [eV]	LUMO[e], (theo.)[d] [eV]	$J_{sc}^{TiO_2}$, J_{sc}^{ZnO} [mA cm^{-2}][f]	$V_{oc}^{TiO_2}$, V_{oc}^{ZnO} [V][f]	FF^{TiO_2}, FF^{ZnO}[f]	η^{TiO_2}, η^{ZnO}[f] [%]
DTPA	298, (40 800)	374	6819	+0.36	−5.16, (−4.21)	−1.53, (−1.14)	—	—	—	—
1	364, (18 700)	448	5151	+0.42	−5.22, (−4.38)	−2.16, (−1.86)	0.76	0.63	0.54	0.26
2	376, (17 300)	443	4022	+0.50	−5.30, (−4.53)	−2.31, (−2.05)	2.14, 1.31	0.70, 0.52	0.66, 0.56	0.98, 0.39
3	373, (21 700)	439	4031	+0.56	−5.36, (−4.66)	−2.36, (−2.16)	2.34	0.70	0.45	0.75

[a] In CH_2Cl_2. [b] Half-wave potentials for oxidation ($E_{1/2}^{ox}$) recorded by cyclic voltammetry in CH_2Cl_2 with 0.1 M nBu_4NPF_6 (scan rate 150 mV s^{-1}, referenced *vs.* Fc/Fc^+). [c] HOMO level estimated from $E_{HOMO} = -(E_{1/2}^{ox} + 4.8\ eV)$.[27] [d] Orbital energies calculated at the OLYP/6-311+G(d,p)//ωB97XD/6-31G(d) level of theory. [e] LUMO level estimated from $E_{LUMO} = E_{HOMO} + E_g$; optical band gap E_g corresponds to $E_g = 1240\lambda_{max}^{-1}$. [f] Photocurrent–voltage characteristics measured under simulated solar light conditions (1 sun and AM 1.5 conditions).

and 0.70 for **2** and **3**. The low FFs noted for devices with **1** are quite likely due to the poor surface coverage, which is indicative for efficient electron recombination processes from the TiO_2 electrode to the electrolyte. As a consequence, the electron density in the electrode is reduced, especially for devices with **1**, and, in turn, the quasi-Fermi level of the sensitized electrode is lowered. In line with this argument is the fact that the lowest open-circuit voltage (V_{oc}) in this series is noted for devices with **1** (Fig. 4). Our results imply that the binding of only one pyridyl group onto the electrode surface is inefficient, whereas the use of two or three pyridyl groups leads to enhanced device performances. Not surprisingly, the short-circuit current density (J_{sc}) is the lowest for devices with **1**, while devices with **2** feature the highest J_{sc} after 30 h adsorption time followed by a gradual decrease. The latter J_{sc} and subsequently the efficiency values amount to approximately one fourth of the highest reported efficiencies of pyridyl-based DSSCs up to date.[14–20] Finally, devices with **3** show decreasing J_{sc} with the adsorption time. This finding is likely to be due to aggregation on the electrode surface, as already shown in similar systems.[3,13–15]

In the next step, the incident-photon-to-current-efficiency (IPCE) spectra of the different devices were analyzed. Particular emphasis is placed on confirming the aforementioned trends for J_{sc} as a means to highlight the role of **1–3** as sensitizers (see Fig. 5). In detail, the IPCE spectra show a rising band at around 400 nm as a function of adsorption time. Maximum values are 23.1%, 58.4%, and 62.3% for devices with **1**, **2**, and **3**, respectively (Fig. 5, see also ESI Fig. S15 and S16†). Overall, our data indicate that devices containing **2** with an efficiency (η) of 0.98% outperform those with **1** or **3**.

To clarify the observed differences between the devices containing **2** and **3**, the stability of them adsorbed onto TiO_2-based electrodes was studied under constant irradiation (AM 1.5 and 1 sun) and thermal treatment (from room temperature to 300 °C with 50 °C steps each for 30 minutes). From UV/vis spectroscopy we infer that both dyes are stable for at least 90 minutes under constant irradiation and heating of up to 200 °C. Following that substantial changes with respect to the shape of the absorption spectra occurred (Fig. S18†). It is unlikely that a lack of dye stability is compromised and causes the observed device differences. Instead, one of the three pyridyl groups in **3**, which remains unshielded from the electrolyte, is the inception for possible interactions with the redox electrolyte. To follow up on this notion, UV/vis absorption and emission spectroscopic assays were performed for **1–3** both in solution and with sensitized TiO_2-based electrodes. To this end, a strong emission quenching was observed in ethanol solution upon electrolyte addition (Fig. S19†), suggesting a fast deactivation pathway through the population of the triplet excited state due to heavy atom effects. Simultaneously, a hypsochromic shift of the lowest-energy band sets in and a new band develops at around 300 nm (Fig. S20†). No shifts were, however, observed when the same experiments were performed with sensitized TiO_2-based electrodes (Fig. S13 and S18†). Moreover, the IPCE data for **1–3** are the same and match perfectly the absorption features of the sensitized TiO_2-based electrodes. It is reasonable to conclude that in a device under working conditions no significant interactions between the pyridyl linkers and the electrolyte takes place. Taking the aforementioned into concert, the most likely rationale for the differences between the devices containing **2** and **3** is the adsorption motif and/or arrangement at the electrode surface due to the unbound pyridyls.

Finally, **2** was used as probe to shed light onto the impact of the electrode material on the device performance. To this end, devices with ZnO-based electrodes featuring similar nanoparticle size and thickness as those used for the above-mentioned experiments with TiO_2-based DSSCs were fabricated (for experimental details, see ESI†). In this context, the basicity

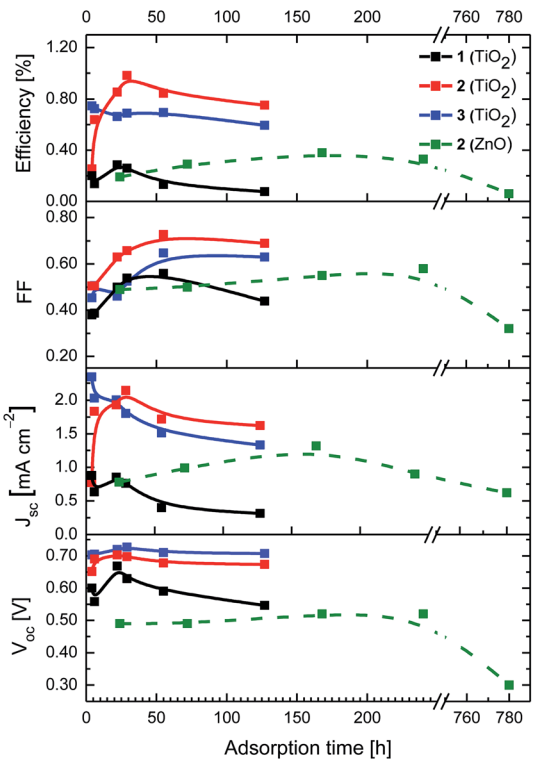

Fig. 4 Figures-of-merit of DSSCs based on TiO_2 electrodes with **1–3** (solid lines) and ZnO electrodes with **2** (dashed lines) at different adsorption times.

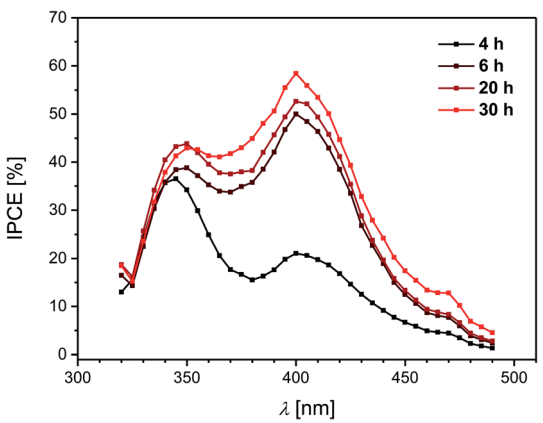

Fig. 5 IPCE spectra of TiO_2-based DSSCs with **2** at different adsorption times.

of ZnO films and the weak Zn–pyridine bond resulted in sluggish adsorption kinetics when compared to TiO_2-based electrodes (Fig. 4).[29] As such, the figures-of-merits for ZnO-based devices continuously grow until an adsorption time of 200 h is reached. Here, a maximum overall efficiency of 0.39% is realized (Fig. 4). Longer immersion times lead to a reduction of FF and J_{sc}, which might be ascribed to aggregation rather than to the intrinsic electrode instability.[2c,30]

Conclusions

In conclusion, we have synthesized a new family of fluorescent organic electron donor–acceptor dyes composed of a central *N*-heterotriangulene as electron donor decorated with 4-pyridyls as electron-withdrawing anchors and incorporated them as sensitizers in n-type DSSCs featuring TiO_2 and ZnO electrodes. A combination of spectroscopic, electrochemical, and theoretical investigations assisted in documenting that as the number of pyridyl units is increased the HOMO as well as LUMO energies decreased. From absorption and emission assays we concluded pronounced solvatochromism and significant bathochromic shifts upon protonation. The latter feature bears great potential for fluorescent pH sensors. Moreover, we demonstrated that the pyridyl anchors in these novel electron donor–acceptor dyes enable, on one hand, the adsorption onto TiO_2- and ZnO-based electrodes and, on the other hand, the effective electron injection upon light irradiation. In this context, the best device performances were realized with the dye that bears two pyridyl anchors. The latter seems to provide a good balance between efficient binding to the metal oxide surface and suppressing self-aggregation once immobilized onto the electrode surface. We are confident about future DSSC performance improvement by introduction of additional π-conjugated spacers, such as thiophenes, between the *N*-heterotriangulene core and the pyridyl anchors. This is primarily meant to enhance the absorption properties and, in turn, the light harvesting/photon collection characteristics.

Acknowledgements

This work was supported by the "Solar Technologies Go Hybrid" (SolTech) initiative of the Free State of Bavaria. The German Research Foundation (DFG) through the Collaborative Research Center SFB 953 "Synthetic Carbon Allotropes", the Cluster of Excellence "Engineering of Advanced Materials" (EAM) at the Friedrich-Alexander University (FAU) Erlangen-Nürnberg, and the Graduate School Molecular Science (GSMS) of FAU Erlangen-Nürnberg are gratefully acknowledged for their generous support.

Notes and references

1 (*a*) B. O'Regan and M. Grätzel, *Nature*, 1991, **353**, 737–740; (*b*) M. Grätzel, *Nature*, 2001, **414**, 338–344.

2 (*a*) A. Hagfeldt, G. Boschloo, L. Sun, L. Kloo and H. Pettersson, *Chem. Rev.*, 2010, **110**, 6595–6663; (*b*) J. A. Anta, E. Guillén and R. Tena-Zaera, *J. Phys. Chem. C*, 2012, **116**, 11413–11425; (*c*) R. D. Costa, F. Lodermeyer, R. Casillas and D. M. Guldi, *Energy Environ. Sci.*, 2014, **7**, 1281–1296; (*d*) F. Bella, C. Gerbaldi, C. Barolo and M. Grätzel, *Chem. Soc. Rev.*, 2015, **44**, 3431–3473; (*e*) M. Ye, X. Wen, M. Wang, J. Iocozzia, N. Zhang, C. Lin and Z. Lin, *Mater. Today*, 2015, **18**, 155–162.

3 (*a*) A. Mishra, M. K. R. Fischer and P. Bäuerle, *Angew. Chem., Int. Ed.*, 2009, **48**, 2474–2499; (*b*) M. Urbani, M. Grätzel, M. K. Nazeeruddin and T. Torres, *Chem. Rev.*, 2014, **114**, 12330–12396; (*c*) C.-P. Lee, R. Y.-Y. Lin, L.-Y. Lin, C.-T. Li, T.-C. Chu, S.-S. Sun, J. T. Lin and K.-C. Ho, *RSC Adv.*, 2015, **5**, 23810–23825; (*d*) J. Wu, Z. Lan, J. Lin, M. Huang, Y. Huang, L. Fan and G. Luo, *Chem. Rev.*, 2015, **115**, 2136–2173; (*e*) M.-E. Ragoussi and T. Torres, *Chem. Commun.*, 2015, **51**, 3957–3972.

4 A. Listorti, B. O'Regan and J. R. Durrant, *Chem. Mater.*, 2011, **23**, 3381–3399.

5 (*a*) L. Schmidt-Mende, U. Bach, R. Humphry-Baker, T. Horiuchi, H. Miura, S. Ito, S. Uchida and M. Grätzel, *Adv. Mater.*, 2005, **17**, 813–815; (*b*) S. Ito, S. M. Zakeeruddin, R. Humphry-Baker, P. Liska, R. Charvet, P. Comte, M. K. Nazeeruddin, P. Péchy, M. Takata, H. Miura, S. Uchida and M. Grätzel, *Adv. Mater.*, 2006, **18**, 1202–1205; (*c*) D. Kuang, S. Uchida, R. Humphry-Baker, S. M. Zakeeruddin and M. Grätzel, *Angew. Chem., Int. Ed.*, 2008, **47**, 1923–1927; (*d*) S. Ito, H. Miura, S. Uchida, M. Takata, K. Sumioka, P. Liska, P. Comte, P. Péchy and M. Grätzel, *Chem. Commun.*, 2008, 5194–5196.

6 (*a*) S. Wang, J. Guo, L. He, H. Wang, J. Zhao and C. Lu, *Synth. Met.*, 2013, **168**, 1–8; (*b*) C. A. Richard, Z. Pan, H.-Y. Hsu, S. Cekli, K. S. Schanze and J. R. Reynolds, *ACS Appl. Mater. Interfaces*, 2014, **6**, 5221–5227.

7 K. Guo, K. Yan, X. Lu, Y. Qiu, Z. Liu, J. Sun, F. Yan, W. Guo and S. Yang, *Org. Lett.*, 2012, **14**, 2214–2217.

8 (*a*) S. Franco, J. Garín, N. M. de Baroja, R. Pérez-Tejada, J. Orduna, Y. Yu and M. Lira-Cantú, *Org. Lett.*, 2012, **14**, 752–755; (*b*) R. Pérez-Tejada, N. M. de Baroja, S. Franco, L. Pellejà, J. Orduna, R. Andreu and J. Garín, *Dyes Pigm.*, 2015, **123**, 293–303.

9 (*a*) Z. Ning and H. Tian, *Chem. Commun.*, 2009, 5483–5495; (*b*) M. Liang and J. Chen, *Chem. Soc. Rev.*, 2013, **42**, 3453–3488.

10 (*a*) W.-H. Liu, I.-C. Wu, C.-H. Lai, C.-H. Lai, P.-T. Chou, Y.-T. Li, C.-L. Chen, Y.-Y. Hsu and Y. Chi, *Chem. Commun.*, 2008, 5152–5154; (*b*) J.-H. Yum, D. P. Hagberg, S.-J. Moon, K. M. Karlsson, T. Marinado, L. Sun, A. Hagfeldt, M. K. Nazeeruddin and M. Grätzel, *Angew. Chem., Int. Ed.*, 2009, **48**, 1576–1580.

11 (*a*) D. Hellwinkel and M. Melan, *Chem. Ber.*, 1971, **104**, 1001–1016; (*b*) J. E. Field and D. Venkataraman, *Chem. Mater.*, 2002, **14**, 962–964.

12 (*a*) D. Kim, C. Kim, H. Choi, K. Song, M.-S. Kang and J. Ko, *J. Photochem. Photobiol., A*, 2011, **219**, 122–131; (*b*) L. Cai, H. N. Tsao, W. Zhang, L. Wang, Z. Xue, M. Grätzel and B. Liu, *Adv. Energy Mater.*, 2013, **3**, 200–205; (*c*) F. Wu, H. Liu, L. T. L. Lee, T. Chen, M. Wang and L. Zhu, *Chin. J. Chem.*, 2015, **33**, 925–933; (*d*) F. Wu, L. T. L. Lee, J. Liu,

S. Zhao, T. Chen, M. Wang, C. Zhong and L. Zhu, *Synth. Met.*, 2015, **205**, 70–77.

13 L. Zhang and J. M. Cole, *ACS Appl. Mater. Interfaces*, 2015, **7**, 3427–3455.

14 Y. Ooyama, S. Inoue, T. Nagano, K. Kushimoto, J. Ohshita, I. Imae, K. Komaguchi and Y. Harima, *Angew. Chem., Int. Ed.*, 2011, **50**, 7429–7433.

15 Y. Harima, T. Fujita, Y. Kano, I. Imae, K. Komaguchi, Y. Ooyama and J. Ohshita, *J. Phys. Chem. C*, 2013, **117**, 16364–16370.

16 (*a*) Y. Ooyama, T. Nagano, S. Inoue, I. Imae, K. Komaguchi, J. Ohshita and Y. Harima, *Chem.–Eur. J.*, 2011, **17**, 14837–14843; (*b*) Y. Ooyama, N. Yamaguchi, I. Imae, K. Komaguchi, J. Ohshita and Y. Harima, *Chem. Commun.*, 2013, **49**, 2548–2550; (*c*) Y. Ooyama, K. Uenaka, M. Kanda, T. Yamada, N. Shibayama and J. Ohshita, *Dyes Pigm.*, 2015, **122**, 40–45; (*d*) Y. Ooyama, K. Uenaka and J. Ohshita, *Eur. J. Org. Chem.*, 2015, 3713–3720; (*e*) Y. Harima, Y. Kano, T. Fujita, I. Imae, Y. Ooyama and J. Ohshita, *RSC Adv.*, 2015, **5**, 71387–71392.

17 (*a*) D. Daphnomili, G. Landrou, S. P. Singh, A. Thomas, K. Yesudas, K. Bhanuprakash, G. D. Sharma and A. G. Coutsolelos, *RSC Adv.*, 2012, **2**, 12899–12908; (*b*) D. Daphnomili, G. D. Sharma, S. Biswas, K. R. J. Thomas and A. G. Coutsolelos, *J. Photochem. Photobiol., A*, 2013, **253**, 88–96; (*c*) J. Lu, X. Xu, Z. Li, K. Cao, J. Cui, Y. Zhang, Y. Shen, Y. Li, J. Zhu, S. Dai, W. Chen, Y. Cheng and M. Wang, *Chem.–Asian J.*, 2013, **8**, 956–962; (*d*) C. Stangel, A. Bagaki, P. A. Angaridis, G. Charalambidis, G. D. Sharma and A. G. Coutsolelos, *Inorg. Chem.*, 2014, **53**, 11871–11881.

18 Y. Ooyama, Y. Hagiwara, T. Mizumo, Y. Harima and J. Ohshita, *New J. Chem.*, 2013, **37**, 2479–2485.

19 M. Cheng, X. Yang, J. Li, C. Chen, J. Zhao, Y. Wang and L. Sun, *Chem.–Eur. J.*, 2012, **18**, 16196–16202.

20 (*a*) B. Jin, W. Wu, X. Zhang, F. Guo, Q. Zhang and J. Hua, *Chem. Lett.*, 2013, **42**, 1271–1272; (*b*) M.-D. Zhang, H.-X. Xie, X.-H. Ju, L. Qin, Q.-X. Yang, H.-G. Zheng and X.-F. Zhou, *Phys. Chem. Chem. Phys.*, 2013, **15**, 634–641; (*c*) J. Mao, D. Wang, S.-H. Liu, Y. Hang, Y. Xu, Q. Zhang, W. Wu, P.-T. Chou and J. Hua, *Asian J. Org. Chem.*, 2014, **3**, 153–160; (*d*) Y. Ooyama, K. Uenaka, T. Sato, N. Shibayama and J. Ohshita, *RSC Adv.*, 2015, **5**, 2531–2535.

21 (*a*) S. Gottardi, K. Müller, J. C. Moreno-López, H. Yildrim, U. Meinhardt, M. Kivala, A. Kara and M. Stöhr, *Adv. Mater. Interfaces*, 2014, **1**, 1300025; (*b*) A. T. Haedler, S. R. Beyer, N. Hammer, R. Hildner, M. Kivala, J. Köhler and H.-W. Schmidt, *Chem.–Eur. J.*, 2014, **20**, 11708–11718; (*c*) N. Hammer, T. A. Schaub, U. Meinhardt and M. Kivala, *Chem. Rec.*, 2015, **15**, 1119–1131; (*d*) A. T. Haedler, K. Kreger, A. Issac, B. Wittmann, M. Kivala, N. Hammer, J. Köhler, H.-W. Schmidt and R. Hildner, *Nature*, 2015, **523**, 196–199; (*e*) J.-C. Moreno-López, S. Gottardi, U. Meinhardt, H. Yildrim, A. Kara, M. Kivala and M. Stöhr, *Chem.–Eur. J.*, 2016, **22**, 581–589; (*f*) C. Steiner, B. D. Gliemann, U. Meinhardt, M. Gurrath, B. Meyer, M. Kivala and S. Maier, *J. Phys. Chem. C*, 2015, **119**, 25945–25955.

22 Z. Fang, T.-L. Teo, L. Cai, Y.-H. Lai, A. Samoc and M. Samoc, *Org. Lett.*, 2009, **11**, 1–4.

23 F. Schlütter, F. Rossel, M. Kivala, V. Enkelmann, J.-P. Gisselbrecht, P. Ruffieux, R. Fasel and K. Müllen, *J. Am. Chem. Soc.*, 2013, **135**, 4550–4557.

24 L. M. Salonen, M. Ellermann and F. Diederich, *Angew. Chem., Int. Ed.*, 2011, **50**, 4808–4842.

25 P. Suppan, *J. Photochem. Photobiol., A*, 1990, **50**, 293–330.

26 B. Hu, X. Chen, Y. Wang, P. Lu and Y. Wang, *Chem.–Asian J.*, 2013, **8**, 1144–1151.

27 J. Pommerehne, H. Vestweber, W. Guss, R. F. Mahrt, H. Bässler, M. Porsch and J. Daub, *Adv. Mater.*, 1995, **7**, 551–554.

28 *Energy Efficiency and Renewable Energy Through Nanotechnology*, ed. L. Zang, Springer, 2011.

29 (*a*) St. Hövel, C. Kolczewski, M. Wühn, J. Albers, K. Weiss, V. Staemmler and C. Wöll, *J. Chem. Phys.*, 2000, **112**, 3909–3916; (*b*) P. Joshi, V. Shewale, R. Pandey, V. Shanker, S. Hussain and S. P. Karna, *Phys. Chem. Chem. Phys.*, 2011, **13**, 476–479.

30 J. Wu and D. Xue, *Sci. Adv. Mater.*, 2011, **3**, 127–149.